World Academy of Science, Engineering and Technology
International Journal of Electronics and Communication Engineering
Vol:12, No:10, 2018

Implementation the Average Input Current Mode Control of Two-Phase Interleaved Boost Converter Using Low-Cost Microcontroller

Yin Yin Phyo, Tun Lin Naing

***Abstract*—**In this paper, the average input current mode control is proposed for two-phase interleaved boost converter with two separate input inductors operating in continuous conduction mode (CCM). The required mathematical model is obtained from the equivalent circuits of its different four modes of operation. The small ripple approximation is derived to find the transfer functions from dynamic model using switching function. In average input current mode control, the inner current loop and outer voltage loop are designed with PI controller using bode analysis. Anti-windup structure is applied for PI controllers in control system. Moreover, the simulation work is carried out by MATLAB/Simulink. And, the hardware prototype is implemented by using low-cost microcontroller Arduino Nano. Finally, the laboratory prototype, available from the local market, is constructed to validate the mathematical model. The results show that the output voltage response is the faster rise time and settling time with acceptable overshoot.

***Keywords*—**Average input current mode control, interleaved boost converter, low-cost microcontroller, PI controller, switching function.

I. Introduction

IN recent years, DC-DC converters are widely used in many applications such as DC drives, computer power supply, renewable energy source and automotive, power factor correction and so on [1]-[3]. But, the conventional boost converter has many disadvantages such as the large output capacitor required to reduce the ripple voltage, larger input current ripple and poor efficiency. Interleaved topology is used to solve this problem. There are many methods to analyze the converters. Banerjee et al. [4] presented the two-phase IBC without considering all parasitic elements to find the transfer function from the state-space averaging technique. But, the state-space averaging method is sometimes complex when the converter circuit contains many elements. Therefore, the signal flow graph (SFG) nonlinear graphical modeling method was developed for PWM converter to solve the above problem in [5]. But, these methods are complex and many mathematical equations are needed.

The IBC has right-half plane zero (RHPZ) in output voltage to control transfer function. But, transfer functions of inductor current for two-phase IBC do not have the RHPZ. RHPZ zero can cause the system step-response slower and make the response reversed overshoot. The input current is high during starting although the output voltage is regulated in voltage mode control [6]. Therefore, the current mode method is important in order to avoid these effects. There are many current mode control methods such as average current mode control, peak current control and slope current control. Among them, average current mode control method is proposed in this paper because this method is easily to compensate the system.

Fellipe [7] studied the six-phase interleaved double dual boost converter and the output is controlled using current mode control. The output of voltage controller is used as the reference of current loop (internal loop). Kolluri and Narasamma [8] presented the average current mode control for two-phase IBC using independent current loops and then realized the controller using three OPA606 op-amps, three SG3524 modulator ICs. Chen et al. [9] proposed decoupled current-balancing control (DCBC) with the voltage-regulating loop and current balancing loop are parallel for two-phase IBC.

Two current sensors are required to implement current balancing function for two-phase IBC [10]-[12]. The current sensing is an important function for current control of the converter. Some papers proposed several circuit topologies and control schemes to reduce the number of current sensors [8], [13]. Moreover, many control methods are proposed in [14]-[18], such as voltage mode control, current mode control, sliding mode control, predictive control, one-cycle control and so on. These proposed control methods are used to improve the voltage regulation. The controller designs of these methods are more complicated, although their performance is good.

The first objective of this paper is to derive the transfer function from small-signal analysis using dynamic model with switching function. This approach is distinct from other methods [4], [5]. This method is easier to achieve the transfer function with minimum mathematical equations.

The second objective is to implement the average input current mode control of a two-phase IBC using low-cost microcontroller as described in [19], [20]. In this regard, this paper proposes the low-cost microcontroller Arduino Nano. There are many reasons for using it. Firstly, it is small, cheap and compact. Secondly, the use of software programming and hardware implementation is easily understood and friendly than the other microcontrollers. Thirdly, it can be easily obtained from the market in Myanmar.

The remaining sections of this paper are described as

Yin Yin Phyo is with the Mandalay Technological University, Mandalay, Myanmar (e-mail: yinyinphyo2000@gmail.com).

Tun Lin Naing is with the Department of Electrical Power Engineering, Mandalay Technological University, Mandalay, Myanmar (e-mail: tunlinnaing1980@gmail.com).

follows: The mathematical modeling of two-phase IBC is described in Section II. The PI controller gains for inner current loop and outer voltage loop are calculated in Section III. Simulation and experimental results are discussed in Sections IV and V. Finally, this paper is concluded in Section VI.

II. Mathematical Modeling of Two-Phase Interleaved Boost Converter

The two-phase interleaved boost converter with control scheme is illustrated in Fig. 1. The two-phase IBC consists of separate input inductors L_1 and L_2, switches S_1 and S_2, diodes D_1 and D_2 and the same filter capacitor C at the output. The switches S_1 and S_2 have the same switching frequency. The load is represented by a resistor R. The inductor stored and released energy when the switch is ON and OFF. The capacitor is used for filtering the ripple in the output voltage V_o. The gate signals of switches S_1 and S_2 are represented by u_1 and u_2. The possible values of gate switches are $u_1 \in \{0,1\}$ and $u_2 \in \{0,1\}$, in which 0 and 1 represent OFF and ON states of the power switches. And, the gate signals u_1 and u_2 are shifted by 180 degrees.

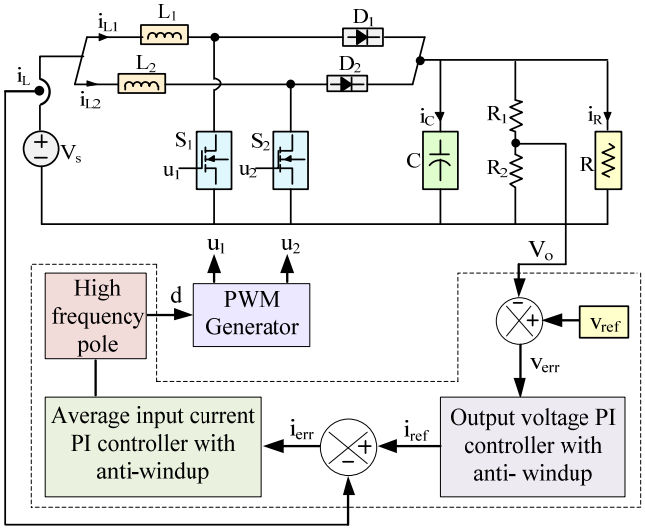

Fig. 1 Circuit diagram of two-phase IBC with control scheme

In proposed control scheme, outer voltage loop and inner current loop are contained. PI controller with anti-windup is designed for both control loops. The input voltage range of microcontroller is 0-5 V. Therefore, it is needed to reduce the converter output voltage. R_1 and R_2 are applied to solve the problem by using the voltage divider method. It helps send the converter output voltage to the microcontroller. The reference current (i_{ref}) is the output signal of voltage controller and the duty cycle (d) is the output signal of current controller. This duty cycle is used to generate the PWM signal. These PWM signals are fed into the gates of the switches u_1 and u_2.

A. Switched-Function Model

The system has four logics because the gate signals of u_1 and u_2 have two states (i.e. 0 and 1). Therefore, the system operates in four modes. The inductor resistance is considered in this paper but the parasitic elements such as MOSFET ON resistance, diode voltage drop and capacitor parasitic resistance are not considered. The converter is assumed as operating in CCM. Also, it can be assumed that the values of separate input inductors L_1 and L_2 are identical. The equivalent circuits of four modes are shown as the following figures.

Mode 1: u_1=1 and u_2=0. Fig. 2 illustrates the equivalent circuit of mode 1.

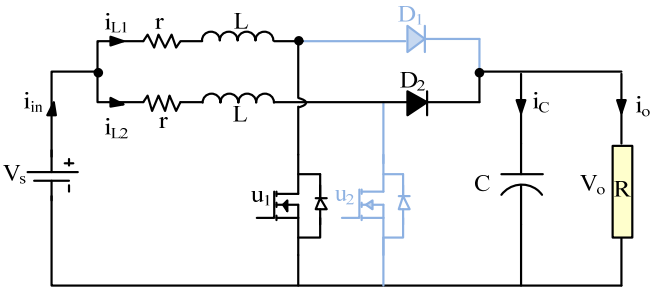

Fig. 2 Equivalent circuit for Mode 1

For equivalent circuit of Mode 1, the following differential equations are obtained by applying *Kirchhoff's voltage and current laws.*

$$L\frac{di_{L1}}{dt} = V_s - ri_{L1} \tag{1}$$

$$L\frac{di_{L2}}{dt} = V_s - ri_{L2} - v_o \tag{2}$$

$$C\frac{dv_o}{dt} = i_{L2} - \frac{v_o}{R} \tag{3}$$

Mode 2: u_1=0 and u_2=1. Fig. 3 shows the equivalent circuit of mode 2.

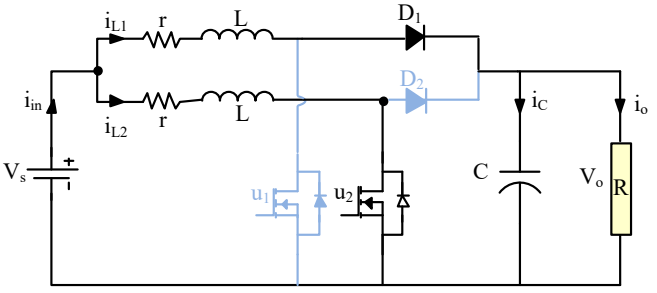

Fig. 3 Equivalent circuit for Mode 2

For equivalent circuit of Mode 2, the following differential equations are obtained by applying *Kirchhoff's voltage and current laws.*

$$L\frac{di_{L1}}{dt} = V_s - ri_{L1} - v_o \tag{4}$$

$$L\frac{di_{L2}}{dt} = V_s - ri_{L2} \tag{5}$$

$$C\frac{dv_o}{dt} = i_{L1} - \frac{v_o}{R} \tag{6}$$

Mode 3: u_1=u_2=1. Fig. 4 illustrates the equivalent circuit of mode 3.

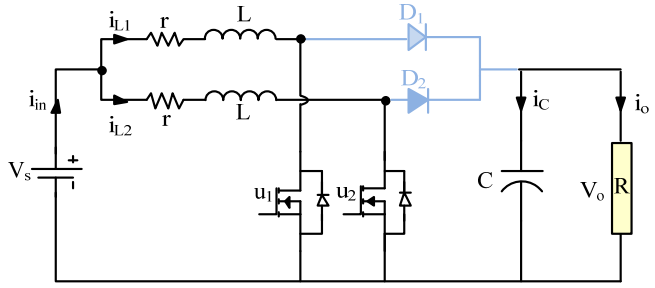

Fig. 4 Equivalent circuit for Mode 3

For equivalent circuit of Mode 3, the following differential equations are obtained by applying *Kirchhoff's voltage and current laws*.

$$L\frac{di_{L1}}{dt} = V_s - ri_{L1} \tag{7}$$

$$L\frac{di_{L2}}{dt} = V_s - ri_{L2} \tag{8}$$

$$C\frac{dv_o}{dt} = -\frac{v_o}{R} \tag{9}$$

Mode 4: u_1=u_2=0. Fig. 5 shows the equivalent circuit of mode 4.

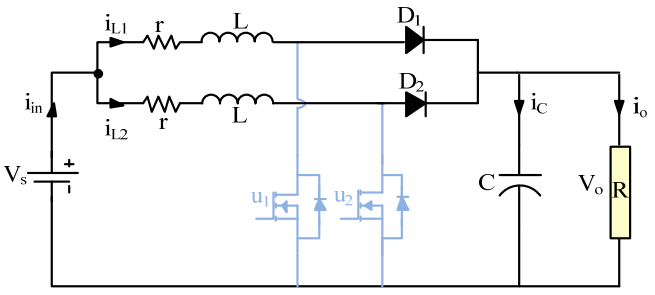

Fig. 5 Equivalent circuit for Mode 4

For equivalent circuit of Mode 4, the following differential equations are obtained by applying *Kirchhoff's voltage and current laws*.

$$L\frac{di_{L1}}{dt} = V_s - ri_{L1} - v_o \tag{10}$$

$$L\frac{di_{L2}}{dt} = V_s - ri_{L2} - v_o \tag{11}$$

$$C\frac{dv_o}{dt} = i_{L1} + i_{L2} - \frac{v_o}{R} \tag{12}$$

The following differential equations are presented by using switched-function.

$$L\frac{di_{L1}}{dt} = V_s - ri_{L1} - (1-u_1)v_o \tag{13}$$

$$L\frac{di_{L2}}{dt} = V_s - ri_{L2} - (1-u_2)v_o \tag{14}$$

$$C\frac{dv_o}{dt} = (1-u_1)i_{L1} + (1-u_2)i_{L2} - \frac{v_o}{R} \tag{15}$$

B. Steady-State Equations of the System

The average model of the system is used to obtain the steady-state equations. The average positions d_1 and d_2 replace the switch positions u_1 and u_2 in (13)-(15).

$$L\frac{d\bar{i}_{L1}}{dt} = V_s - r\bar{i}_{L1} - (1-d_1)\bar{v}_o \tag{16}$$

$$L\frac{d\bar{i}_{L2}}{dt} = V_s - r\bar{i}_{L2} - (1-d_2)\bar{v}_o \tag{17}$$

$$C\frac{d\bar{v}_o}{dt} = (1-d_1)\bar{i}_{L1} + (1-d_2)\bar{i}_{L2} - \frac{\bar{v}_o}{R} \tag{18}$$

whereas, $\bar{u}_1 = d_1 \in [0,1]$ and $\bar{u}_2 = d_2 \in [0,1]$ are the average positions of the switches. The values of d_1 and d_2 are the addition of average and small signal value.

$$d_1 = D_1 + \tilde{d}_1 \text{ and } d_2 = D_2 + \tilde{d}_2 \tag{19}$$

If $\tilde{d} \ll D$, $\tilde{d}$ is neglected by using small-signal approximation. d_1 and d_2 are equal to D in steady-state condition. Therefore, d_1=d_2=D.

$$0 = V_s - rI_{L1} - (1-D)V_o \tag{20}$$

$$0 = V_s - rI_{L2} - (1-D)V_o \tag{21}$$

$$0 = (1-D)I_{L1} + (1-D)I_{L2} - \frac{V_o}{R} \tag{22}$$

In matrix form, (20)-(22) can be represented as:

$$\begin{pmatrix} r & 0 & (1-D) \\ 0 & r & (1-D) \\ (1-D) & (1-D) & -\frac{1}{R} \end{pmatrix} \begin{pmatrix} I_{L1} \\ I_{L2} \\ V_o \end{pmatrix} = \begin{pmatrix} V_s \\ V_s \\ 0 \end{pmatrix} \tag{23}$$

Equation (24) is derived by using (23) and it represents the steady-state condition of the system.

$$\begin{pmatrix} I_{L1} \\ I_{L2} \\ V_o \end{pmatrix} = \begin{pmatrix} \dfrac{1}{2R(1-D)^2+r} \\ \dfrac{1}{2R(1-D)^2+r} \\ \dfrac{2R(1-D)}{2R(1-D)^2+r} \end{pmatrix} V_s \quad (24)$$

C. Small-Signal Transfer Function

The average model is used to find the transfer function from small-signal analysis. The average value of this system is the addition of large-signal and small-signal value.

$$\frac{d(I_{L1}+\tilde{i}_{L1})}{dt} = \left(\frac{V_s - rI_{L1} - r\tilde{i}_{L1} - V_o - \tilde{v}_o}{L} + \frac{DV_o + D\tilde{v}_o + \tilde{d}V_o + \tilde{d}\tilde{v}_o}{L} \right) \quad (25)$$

$$\frac{d(I_{L2}+\tilde{i}_{L2})}{dt} = \left(\frac{V_s - rI_{L2} - r\tilde{i}_{L2} - V_o - \tilde{v}_o}{L} + \frac{DV_o + D\tilde{v}_o + \tilde{d}V_o + \tilde{d}\tilde{v}_o}{L} \right) \quad (26)$$

$$\frac{d(V_o+\tilde{v}_o)}{dt} = \left(\begin{array}{c} \dfrac{I_{L1}+\tilde{i}_{L1} - DI_{L1} - D\tilde{i}_{L1} - \tilde{d}I_{L1} - \tilde{d}\tilde{i}_{L1}}{C} \\ + \dfrac{I_{L2}+\tilde{i}_{L2} - DI_{L2} - D\tilde{i}_{L2} - \tilde{d}I_{L2} - \tilde{d}\tilde{i}_{L2} - \dfrac{V_o}{R} - \dfrac{\tilde{v}_o}{R}}{C} \end{array} \right) \quad (27)$$

The small-signal model is obtained by neglecting the non-linear and steady-state terms in (25)-(27). In matrix form, the small-signal model can be represented as:

$$\begin{bmatrix} \dfrac{d\tilde{i}_{L1}}{dt} \\ \dfrac{d\tilde{i}_{L2}}{dt} \\ \dfrac{d\tilde{v}_o}{dt} \end{bmatrix} = \begin{bmatrix} -\dfrac{r}{L} & 0 & -\dfrac{D'}{L} \\ 0 & -\dfrac{r}{L} & -\dfrac{D'}{L} \\ \dfrac{D'}{C} & \dfrac{D'}{C} & -\dfrac{1}{RC} \end{bmatrix} \begin{bmatrix} \tilde{i}_{L1} \\ \tilde{i}_{L2} \\ \tilde{v}_o \end{bmatrix} + \begin{bmatrix} \dfrac{V_o}{L} \\ \dfrac{V_o}{L} \\ -\dfrac{(I_{L1}+I_{L2})}{C} \end{bmatrix} \tilde{d} + \begin{bmatrix} \dfrac{1}{L} \\ \dfrac{1}{L} \\ 0 \end{bmatrix} V_s \quad (28)$$

The steady-state value of output voltage (V_o) and inductors current (I_{L1},I_{L2}) from (24) are substituted in (28). The transfer functions of two-phase IBC are obtained from (28) by using Laplace transform. Equation (29) is the transfer functions of two-phase IBC.

$$\begin{bmatrix} \tilde{i}_{L1}(s) \\ \tilde{i}_{L2}(s) \\ \tilde{v}_o(s) \end{bmatrix} = \begin{bmatrix} \dfrac{(2D'RV_s)(RCs+2)}{(2D'^2R+r)(r+Ls+2D'^2R+RLCs^2+RCrs)} \\ \dfrac{(2D'RV_s)(RCs+2)}{(2D'^2R+r)(r+Ls+2D'^2R+RLCs^2+RCrs)} \\ \dfrac{-(2RV_s)(-2D'^2R+r+Ls)}{(2D'^2R+r)(r+Ls+2D'^2R+RLCs^2+RCrs)} \end{bmatrix} \tilde{d}(s) \quad (29)$$

III. Controller Design

The input of the voltage controller is the error between the comparison of reference voltage (V_{ref}) and converter's output voltage (V_o) as shown in Fig. 1. The voltage controller generates the average input current reference (i_{ref}) and the current controller determines the duty cycle (d) value. The converter's parameters are shown in Table I. The desired output voltage (reference voltage) is defined as 24 V. Fig. 6 illustrates the closed-loop control diagram for two-phase IBC.

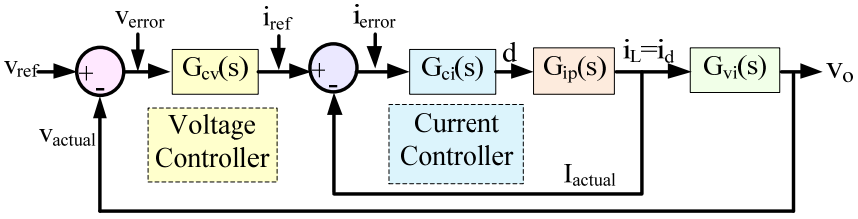

Fig. 6 Closed-loop control system of two-phase IBC

TABLE I
Converter Parameters

Parameters	Variables	Values	Unit
Supply voltage	V_s	12	V
Output voltage	V_o	24	V
Inductors	L_1,L_2	2	mH
Inductor resistance	r	0.2	Ω
Capacitor	C	470	μF
Load Power	P_o	32	W
Load resistance	R	18	Ω
Duty cycle	D	50	%
Switching frequency	f_s	4	kHz

A. Controller Design for Average Current Loop

Fig. 7 shows the block diagram of average input current loop with PI controller. The high frequency pole is included in current controller.

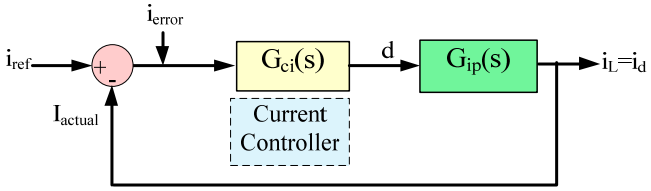

Fig. 7 Block diagram for average current loop control

Control to average current transfer function is calculated from (29) by using converter's parameters of Table I.

$$G_{ip}(s) = \frac{\tilde{i}_L(s)}{\tilde{d}(s)} = \frac{\dfrac{\tilde{i}_{L1}(s)}{\tilde{d}(s)} + \dfrac{\tilde{i}_{L2}(s)}{\tilde{d}(s)}}{2}$$

$$G_{ip}(s)=\frac{1.827s+432}{0.0001557\ s^2+0.03397s+84.64} \tag{30}$$

Equation (30) can be represented as in (31). This equation is obtained from [21].

$$G_{ip}(s)=G_{ip0}\times\frac{1+\frac{s}{\omega_z}}{1+\frac{s}{\omega_0 Q}+\frac{s^2}{\omega_0^2}} \tag{31}$$

where ω_z is the zero frequency, ω_0 is the resonant frequency and Q is the quality factor. The uncompensated current loop gain $G_{ip}(s)$ is equal $T_u(s)$. Therefore,

$$T_u(s)=G_{ip}(s) \tag{32}$$

The bode diagram of control to average input current transfer function is shown in Fig. 8. In bode diagram, the gain margin (G_m) is infinity and phase margin (P_m) 90 degrees. The zero dB crossed frequency is called the cut off frequency (f_c). The cut off frequency of uncompensated control to output voltage transfer function has 2 kHz.

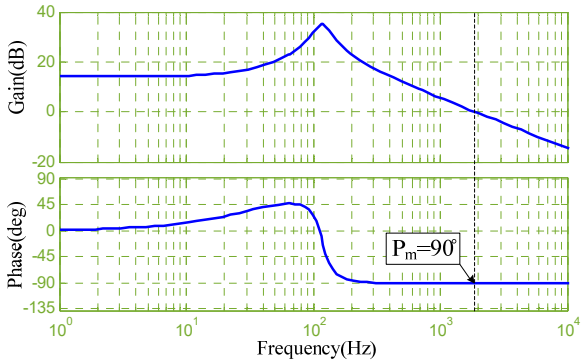

Fig. 8 Bode diagram of uncompensated control to average input current transfer function

The current controller is chosen as a proportional integral (PI) controller. The simple PI compensation law is shown in (33).

$$G_{PI}(s)=G_{PI}(\infty)\left[1+\frac{\omega_{PI}}{s}\right] \tag{33}$$

A high frequency pole is included in compensated transfer function to remove the harmonic content from the switching frequency. The value of high-frequency pole (ω_{HF}) is half of the switching frequency (f_s), that is, at 12566 rad/s. The transfer function of controller is described in (34).

$$G_{ci}(s)=G_{PI}(\infty)\left[1+\frac{\omega_{PI}}{s}\right]\times\frac{1}{1+\frac{s}{\omega_{HF}}} \tag{34}$$

The sample time is defined as 2 ms. In order to calculate the controller gains, cut off frequency (f_c) is equal to the sampling frequency as 500 Hz. The desired phase margin is defined 70 degrees at cut off frequency 500 Hz. The phase lag is added to get the desired phase margin. The phase leg is obtained from (35).

$$tan^{-1}\left(\frac{f_c}{f_{HF}}\right)=tan^{-1}\left(\frac{500}{2000}\right)\approx 14^\circ \tag{35}$$

$$\rho'_m=70^\circ+14^\circ=84^\circ$$

The magnitude and phase of the system uncompensated loop gain are calculated at the target cut off frequency.

$$T_u(j\omega_c)\approx 3.953\Rightarrow 11.9dB$$

$$T_u(j\omega_c)\approx -90^\circ \tag{36}$$

The unknown PI coefficients $G_{PI}(\infty)$ and ω_{PI} are calculated as follows. The value of ω_{PI} is derived based on the required phase margin as shown in (37):

$$-\frac{\pi}{2}+tan^{-1}\left(\frac{\omega_c}{\omega_{PI}}\right)+\angle T_u(j\omega_c)=-\pi+\rho'_m \tag{37}$$

and the value of $G_{PI}(\infty)$ is imposed by the desired cut off frequency in (38):

$$G_{PI}(\infty)\times\sqrt{1+\left(\frac{\omega_c}{\omega_{PI}}\right)^2}\times\left|T_u(j\omega_c)\right|=\frac{\omega_c}{\omega_{PI}} \tag{38}$$

According to (37) and (38), the value of $G_{PI}(\infty)$ and ω_{PI} are 0.252 and 330.25 rad/s. The values of $G_{PI}(\infty)$ and ω_{PI} are substituted in (33).

$$G_{PI}(s)=0.252\left[1+\frac{330.25}{s}\right] \tag{39}$$

If $G_{PI}(s)$ is transformed into ($k_{pi}+k_{ii}/s$), the resulting k_{pi} is found 0.252 and k_{ii} is found 83.233. The compensated control to average input current transfer function is shown in Fig. 9. In bode diagram, the desired phase margin (P_m) is obtained by using these gains. The value of $G_{PI}(\infty)$, ω_{PI} and ω_{HF} are substituted in (34). The compensator transfer function is

$$G_{ci}(s)=\frac{3167s+1.05\times10^6}{s^2+12566s} \tag{40}$$

B. Controller Design for Voltage Loop

The closed-loop control diagram of two-phase IBC for total system is illustrated in Fig. 10.

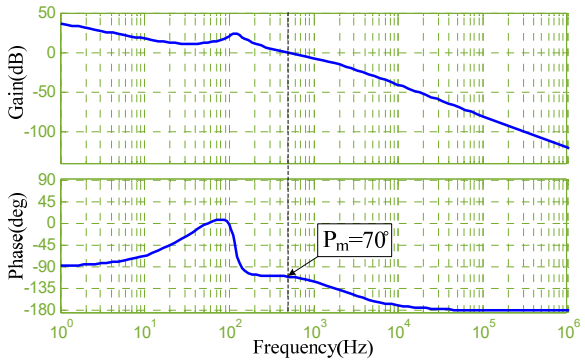

Fig. 9 Bode diagram of compensated open-loop control to average input current transfer function

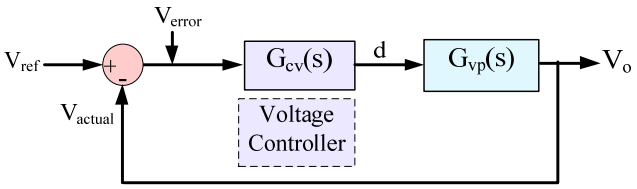

Fig. 10 Block diagram for voltage loop control

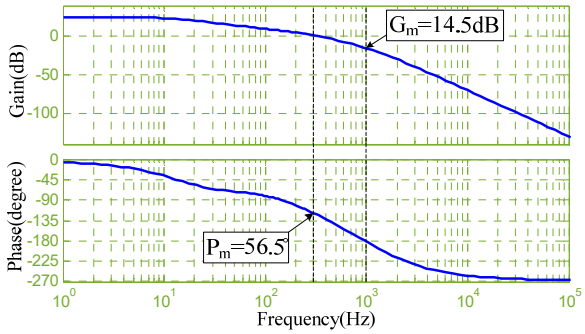

Fig. 11 Bode diagram of uncompensated output voltage to average current reference transfer function

The system transfer function ($\tilde{v}_o(s)/\tilde{i}_{ref}(s)$) with average current loop and voltage to diode transfer function is derived as shown in (41):

$$G_{vp}(s)=\frac{\tilde{v}_o(s)}{\tilde{i}_{ref}(s)}=\frac{\tilde{v}_o(s)}{\tilde{i}_d(s)}\times\frac{\tilde{i}_L(s)}{\tilde{i}_{ref}(s)} \tag{41}$$

The voltage to diode transfer function is

$$G_{vi}(s)=\frac{\tilde{v}_o(s)}{\tilde{i}_d(s)}=\frac{R}{1+RCs} \tag{42}$$

and $\tilde{i}_L(s)/\tilde{i}_{ref}(s)$ is obtained from the closed-loop transfer function of inner average current loop.

The bode plot of output voltage to average current reference transfer function is shown in Fig. 11. In bode diagram, the gain margin (G_m) is found 14.5 dB and phase margin (P_m) is found 56.5 degrees. The cut off frequency of uncompensated output voltage to average current reference transfer function has 300 Hz.

The voltage controller is chosen as a simple proportional integral controller. The PI compensation law is obtained from [20] and described in (43):

$$G_{cv}(s)=G(\infty)\left(1+\frac{\omega_L}{s}\right) \tag{43}$$

In order to calculate the voltage controller gains, the cut off frequency (f_c) is chosen as 20% of sampling frequency. Line frequency (f_L) is taken as 50% of cut off frequency. The magnitude of ω_L is calculated as 314.16 rad/s. According to Fig. 11, gain at 100 Hz is 9.6 dB. $G(\infty)$ is calculated as 0.3311 from:

$$20\log G(\infty)=-9.6dB$$

$G(\infty)$ and ω_L are substituted in (43).

$$G_{cv}(s)=0.3311+\frac{104.02}{s} \tag{44}$$

If $G_{cv}(s)$ is transformed into $(k_{pv}+k_{iv}/s)$ format, the resulting k_{pv} and k_{iv} are found 0.3311 and 104.02. The compensated transfer function is shown in Fig. 12. The system of magnitude and phase are 23.1 dB and 73.6 degrees in bode diagram.

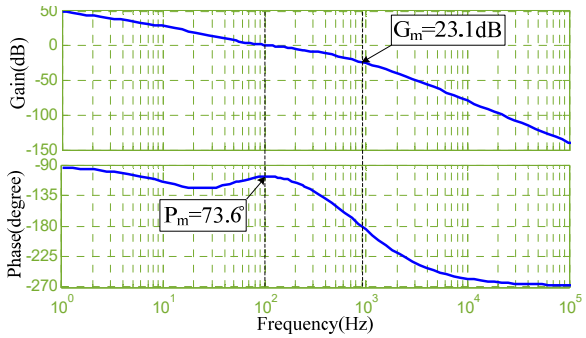

Fig. 12 Compensated open-loop output voltage to average current reference transfer function

Fig. 13 shows the bode diagram of choosing the controller gain based on the sampling frequency. The sample time is very important for the microcontroller. Moreover, the cut off frequency depends on the sampling frequency. In bode diagram, the system response is slow and more oscillating when the cut off frequency is less than the sampling frequency. The smaller cut off frequency means the smaller bandwidth of the system. The smaller bandwidth causes the system step-response slower. Therefore, the cut off frequency is chosen equal to the sampling frequency as 500 Hz in this paper.

Fig. 14 illustrates the bode diagram of overall open-loop transfer function of two-phase IBC with various loads. The value of controller gains is used from Table II. The increasing

of load can cause the system step-response slower and damp according to Fig. 14. When the load is decreased, the system response is faster but more overshoot. Therefore, the rated load resistance is defined 18Ω to find the controller gains. These controller gains are applied for simulation and experiment using anti-windup. The PI controller with anti-windup structure is shown in Fig. 15.

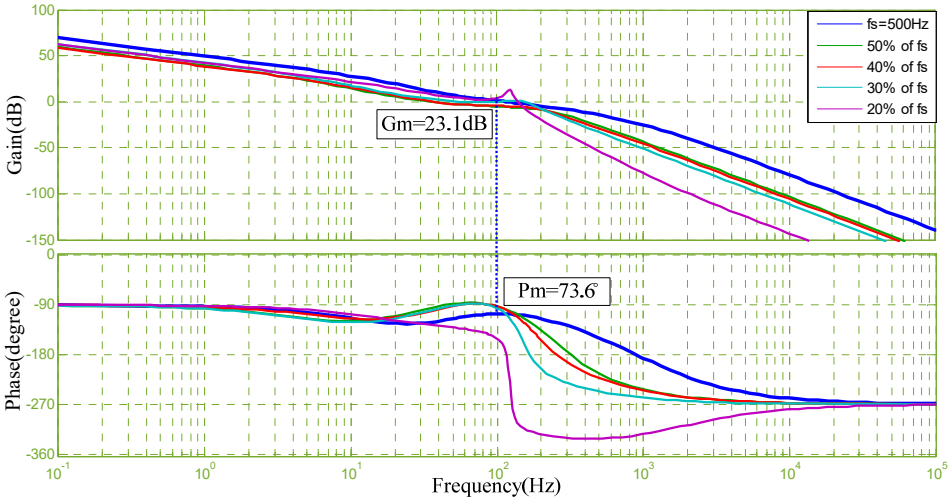

Fig. 13 Bode diagram of choosing the controller gain based on the sampling frequency

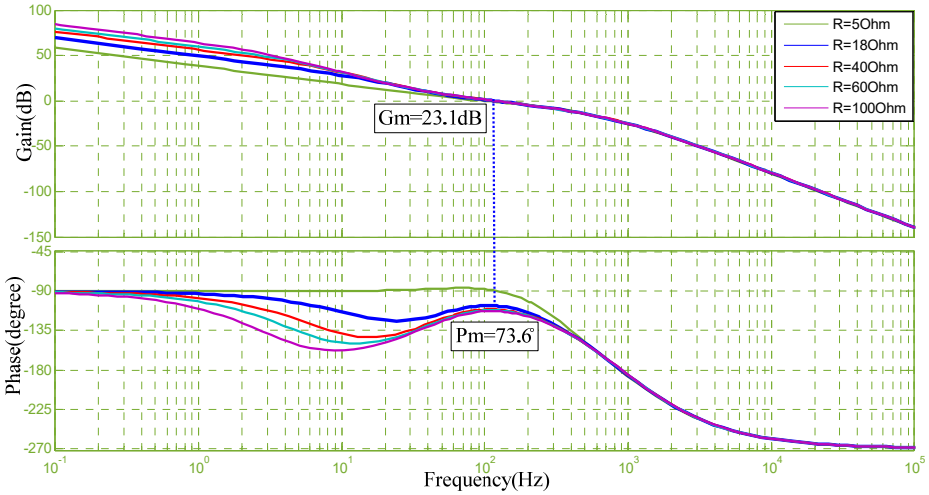

Fig. 14 Bode diagram for compensated overall open-loop transfer function with various loads

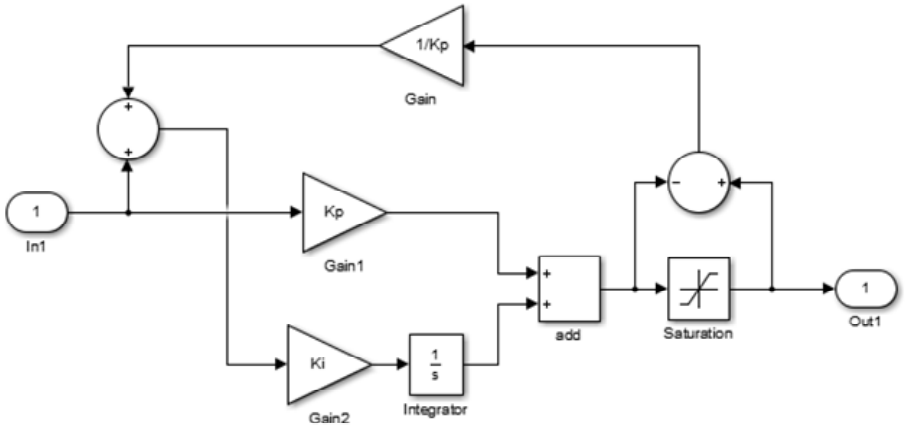

Fig. 15 Simulink blocks of anti-windup structure

There are many methods for anti-windup control. Among them, back calculation method is used in this paper. The output voltage response of converter becomes more overshoot by using a simple PI controller. It can damage the connected load. Therefore, anti-windup control is used to prevent integration part from going too high and instability. The system response achieves better transient performance using PI controller with anti-windup control compared to without anti-windup control for converter [11]. The values of controller gains are described in Table II for current and voltage loop.

TABLE II
CONTROLLER GAINS VALUE

Controller Gains	Values
Current proportional gain, k_{pi}	0.252
Current integral gain, k_{ii}	83.223
Voltage proportional gain, k_{pv}	0.3311
Voltage integral gain, k_{iv}	104.02

IV. SIMULATION RESULTS

The construction of power converter design consumes more time and cost. Simulation study is done to predict the dynamic performances of the system before the actual test. The simulation work is carried out by using MATLAB/Simulink. The simulated transient waveforms of two-phase IBC with input voltage change are shown in Fig. 16 for closed-loop control. The load resistance 24Ω is defined for input voltage changes. The simulation running time is defined as 10 s.

The start-up response of output voltage reached the steady-state condition at 0.1 s and is found a little overshoot about 8.33%. The output voltage (V_{out}) suddenly changed during disturbances but it immediately reached to its set point. The magnitude of input current (I_{in}) is varied under line and load perturbation.

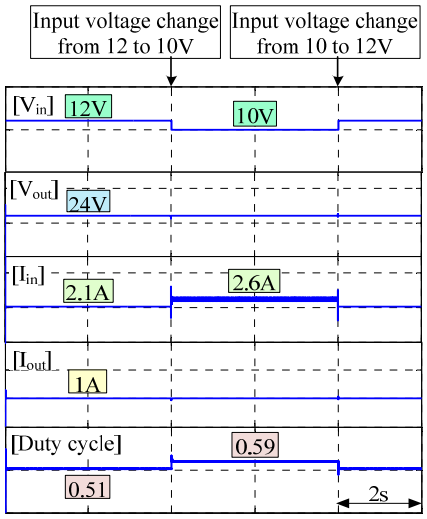

(a)

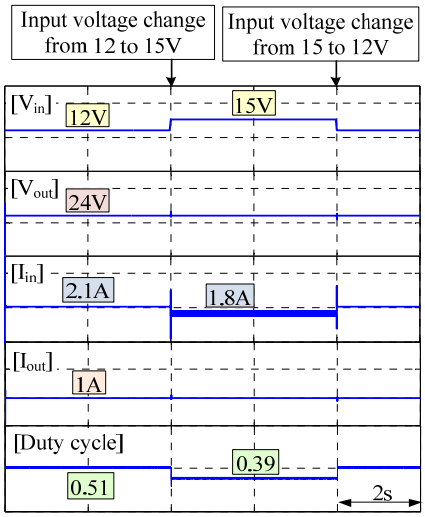

(b)

Fig. 16 Simulated transient waveforms of two-phase IBC with input voltage change from (a) 12 to 10 to 12 V and (b) 12 to 15 to 12 V

Fig. 17 presents the simulated transient waveforms of two-phase IBC with load change for closed-loop test.

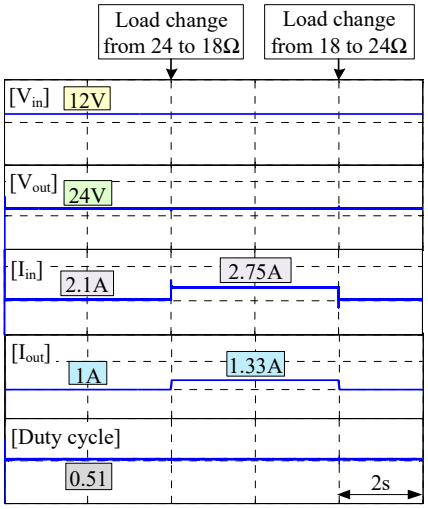

Fig. 17 Simulated transient waveforms of two-phase IBC with load change from 24 to 18 to 24Ω

The magnitude of load current (I_{out}) is constant although the magnitude of input voltage (V_{in}) changed. But, it is varied when the magnitude of load is changed. The magnitude of duty cycle is changed depending on the magnitude of input voltage and load. In Fig. 17, the duty cycle is varied from 0.51 to 0.515 when the magnitude of load is increased from 24 Ω to 18 Ω.

According to the simulation results, it can be found that the output voltage response is constant during disturbances such as line and load perturbation. The practical work is carried out in next section to validate the proposed approach.

V. EXPERIMENT RESULTS

The following results are obtained by using the parameters

listed in Table III. The other parameters are the same as the converter's parameters in Table I.

TABLE III
EXPERIMENTAL PARAMETERS

Parameters	Value/Type
Capacitor	470 µF, 50 V Electrolytic capacitor
Load	24 V, 8 W Lamp
MOSFET	55 V, 49 A, IRF Z44
Diode	800 V, 3 A, BY 399

The proposed two-phase IBC with low-cost microcontroller has been implemented in Fig. 18. The experimental setup of the converter is shown in Fig. 19. Experimental results are generated by using Arduino Nano microcontroller. In experimental setup, the two Arduino Nano boards are used. One board is used as the compensator and another is used as the pwm generator. The compensator generates the pwm and RC low pass filter is used to obtain the duty cycle command.

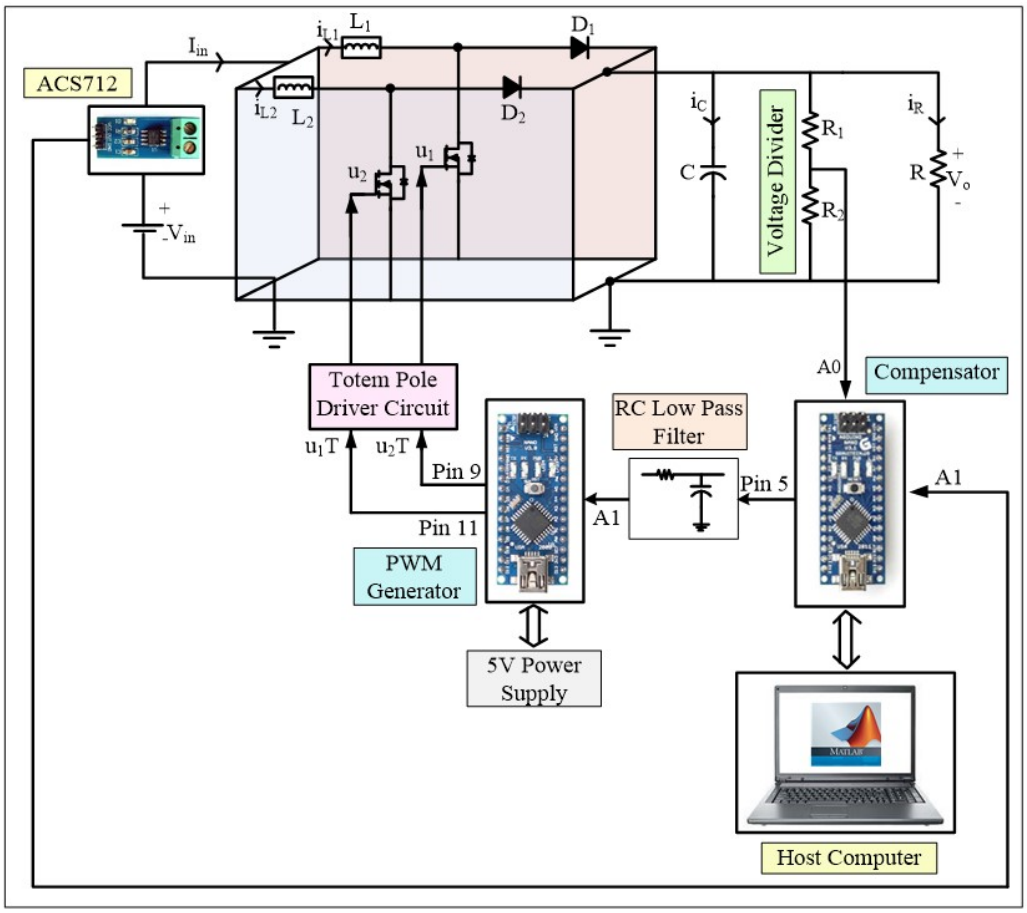

Fig. 18 Hardware setup of two-phase IBC

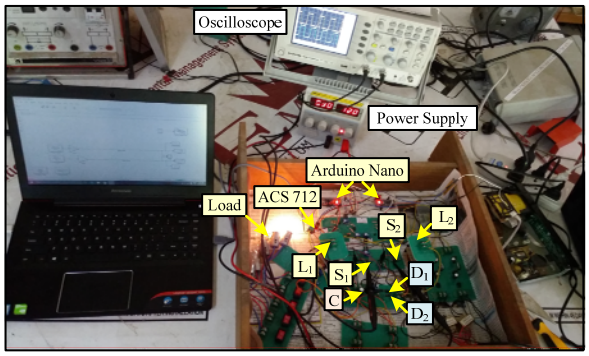

Fig. 19 Experimental setup with Arduino Nano microcontroller

Fig. 20 shows the closed loop control system using MATLAB with Arduino IO package.

The experimental results are obtained by using Arduino IO package and the sampling time is set as 2 ms. Experimental transient waveforms of two-phase IBC with input voltage changes are shown in Fig. 21 for closed-loop control. Fig. 22 illustrates the experimental transient waveforms of two-phase IBC under load perturbation.

The output voltage (V_{out}) response does not dramatically change under line and load perturbation. The input current (I_{in}) suddenly changed from 2.1 to 1.8 A because of increasing the input voltage (V_{in}). When the input voltage is decreased, the input current increased from 2.1 to 2.6 A. Due to the increased load, the input current varied from 2.1 to 2.75 A and the output current (I_{out}) increased from 1 to 1.33 A.

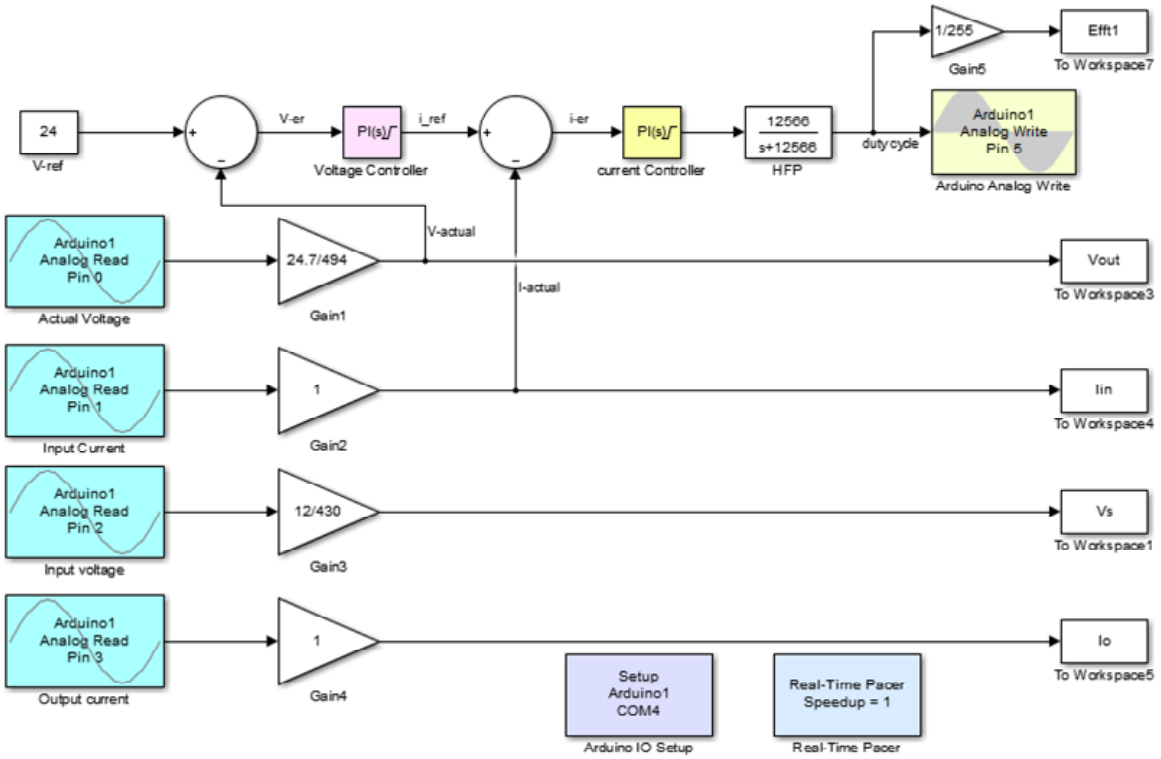

Fig. 20 Simulink model of closed-loop control with Arduino IO library blocks

It is observed that the experimental results are similar to simulation results; the steady-state output voltage is regulated during line and load perturbation. Therefore, the proposed converter gives satisfactory results in the closed-loop system.

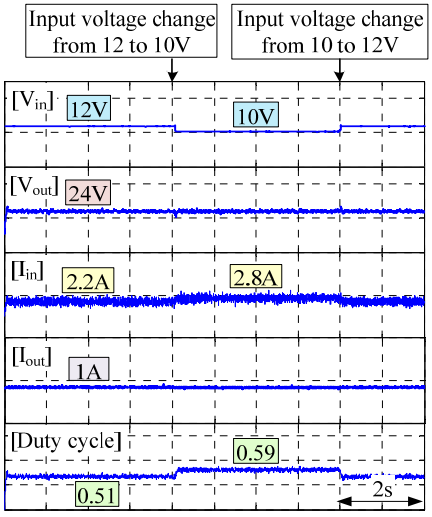

(a)

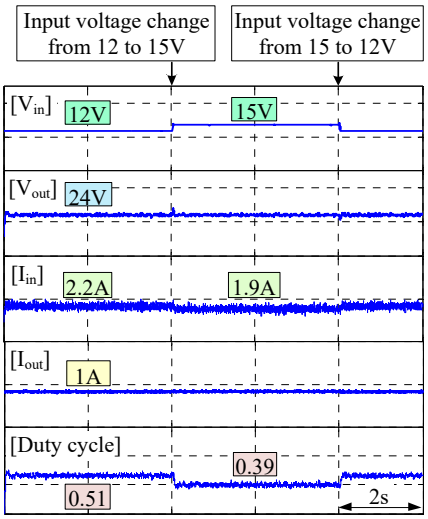

(b)

Fig. 21 Experimental transient waveforms of two-phase IBC with input voltage change from (a) 12 to 10 to 12 V and (b) 12 to 15 to 12 V

VI. Conclusion

This paper presents the proper PI controller design for average input current mode control of two-phase IBC. The experimental results are presented by using low-cost Arduino Nano microcontroller to validate the simulation results. In simulation results, the output voltage response is smooth compared to experimental results. The input current and

output current also have noise in experimental results because of using current sensor. But, the magnitude of the responses in simulation and practical results are nearly the same. It can be concluded that the average input current mode control of two-phase IBC using low-cost Arduino Nano can give the satisfactory response.

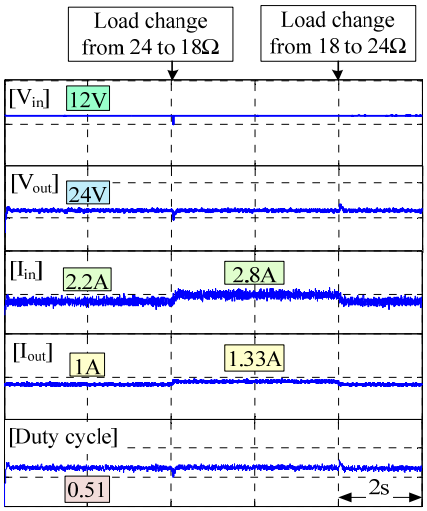

Fig. 22 Experimental transient waveforms of two-phase IBC with load change from 24 to 18 to 24Ω

REFERENCES

[1] Simon Ang, Alejandro Oliva, Power-Switching Converters. Second Edition, Taylor & Francis Group, 2005.
[2] Mohamed Bougrine, M. Benmiloud, A. Benalia, E. Delaleau, M. Benbouzid, "Load Estimator-based Hybrid Controller Design for Two-Interleaved Boost Converter dedicated to Renewable Energy and Automotive applications", ISA Trans, Vol. 66, pp. 425-236, 2016.
[3] Amar Bouafassa, Lazhar Rahmani, Saad Mekhilef, "Design and Real Time Implementation of single phase Boost Power Factor Correction Converter", ISA Trans, Vol 55, Malaysia, 2014, pp. 267-274.
[4] Subrata Banerjee, Arnab Ghosh and Niraj Rana,"Design and Fabrication of Closed Loop Two-Phase Interleaved Boost Converter with Type-III Controller," Industrial Electronics Society (IECON) 42nd Annual Conference of the IEEE, India, 2016, pp. 3331-3336.
[5] Mummadi Veerachary, Tomonobu Senjyu and Katsumi Uezato, "Modeling of closed-loop voltage-mode controlled interleaved dual boost converter," Computers and Electrical Engineering, Vol. 29, Japan, 2003, pp. 67-84.
[6] H. M. Mallikarjuna Swamy, K. P. Guruswamy and Dr. S. P. Singh, "Design and Implementation of Two Phase Interleaved DC-DC Boost Converter with Digital PID Controller," International Journal of Electrical and Electronics Engineering (IJEEE), Vol. 3, India, 2013, pp. 99-104.
[7] Fellipe S. Garcia, Jose A. Pomilio and Giorgio Spiazzi, "Modeling and Control Design of the Interleaved Double Dual Boost Converter," IEEE Trans. Ind. Electronics, Vol. 60, no. 8, pp. 3283-3290, Jun. 2012.
[8] Sandeep Kolluri and Lakshmi Narasamma N, "Analysis, Modeling, Design and Implementation of Average Current Mode Control for Interleaved Boost Converter," Power Electronics and Drive Systems, IEEE 10th International Conference, India, 2013, pp. 280-285.
[9] Hung-Chi Chen, Che-Yu Lu and Li-Ming Huang, "Decoupled Current-Balancing Control with Single-Sensor Sampling-Current Strategy for Two-phase Interleaved Boost-Type Converters," IEEE Trans., Vol. 63, no. 3, pp. 1507-1518, 2016.
[10] R. Saadi, M. Bahri, M.Y. Ayad, M.Becherif, O. Kraa and A. Aboubou,"Implementation and Dual Loop Control of Two Phases Interleaved Boost Converter for Fuel cell Applications," 3rd International Symposium on Environmental Friendly Energies and Applications (EFEA), pp. 1-7, 2014.
[11] X. Huang, T. Nergaard, J.-S. Lai, X. Xu and L. Zhu, "A DSP based controller for high-power interleaved boost converters," in Proc. IEEE Appl. Power Electron. Conf., Vol. 1, pp. 327-333, 2003.
[12] C. Suyong, S. Yujin, P. Sukin and J. Hakgeun, " Digital current sharing method for parallel interleaved dc-dc converters using input ripple voltage," IEEE Trans. Ind. Informat., Vol. 8, no. 3, pp. 536-544, 2012.
[13] Esteban Sanchis, Enrique Maset and Agustin Ferreres, "High-power Battery Discharge Regulator for Space Applications," IEEE Trans. Ind. Electronics, Vol. 57, no.12, Spain, Dec. 2010, pp. 3935-3943.
[14] M. T. Tsai, D. Y. Chen, C. J. Chen, C. H. Chiu and W. H. Chang, "Modeling and design of current balancing control in voltage-mode multiphase interleaved voltage regulators," in Proc. IEEE Int. Power Electron. Conf . (IPEC), pp. 881-887, 2010.
[15] K.-M. Ho, C.-A Yeh and Y.-S. Lai, "Novel digital-controlled transition current-mode control and duty compensation techniques for interleaved power factor corrector," IEEE Trans. Power Electron., Vol. 25, no. 12, pp. 3085-3094, 2010.
[16] Roberto Giral, Luis Martinez-Salamero, Ramon Leyva and Javier Maixe, "Sliding-Mode Control of Interleaved Boost Converter," IEEE Trans. Circuits Syst., Vol. 47, no.9, Spain, 2000, pp. 1330-1339.
[17] C.Sudhakar Babu and M.Veerachary, "Predictive Controller for Interleaved Boost Converter," International Symposium on Industrial Electronics (ISIE), Vol. 2, pp. 577-581, Jun. 2005.
[18] X. Xu, W. Liu and A. Q. Huang, "Two-phase interleaved critical mode PFC boost converter with closed loop interleaving strategy," IEEE Trans. Power Electron., Vol. 24, no. 12, pp. 3003-3013, 2009.
[19] Donny Radianto, Gamal M. Dousoky and Masahito Shoyama, "Design and Implementation of Fast PWM Boost Converter based on Low Cost Microcontroller for Photovoltaic Systems", IEEE Industrial Electronics Society, 41st Annual Conference (IECON), pp. 002324-002328, 2015.
[20] Gokhan Altintas, Mehmet Onur Gulbahce and Derya Ahmet Kocabas, "Nonideal Analysis, Design and Voltage Mode Control of a Boost Converter," Power and Electrical Engineering of Riga Technical University (RTUCON), 57th International Scientific Conference, pp. 1-6, 2016.
[21] Luca Corradini, Dragan Maksimovic, Paolo Mattavelli and Regan Zane, Digital Control of High-Frequency Switched-Mode Power Converters. First Edition, Institute of Electrical and Electronics Engineers, John Wiley & Sons, 2015.